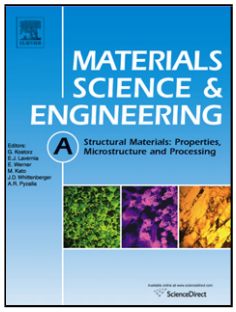

Title: A new constitutive model for HCP metals

Authors: C.Y. Gao, L.C. Zhang, H.X. Yan

PII: S0921-5093(11)00217-6
DOI: doi:10.1016/j.msea.2011.02.053
Reference: MSA 27121

To appear in: *Materials Science and Engineering A*

Received date: 17-10-2010
Revised date: 1-2-2011
Accepted date: 18-2-2011

Please cite this article as: C.Y. Gao, L.C. Zhang, H.X. Yan, A new constitutive model for HCP metals, *Materials Science & Engineering A* (2010), doi:10.1016/j.msea.2011.02.053

- A new constitutive model for HCP metals under coupled high strain, high strain rate and high temperature
- A globally optimal determination of the constitutive parameters in the constitutive equation.
- A more accurate constitutive description of HCP metals than those available in the literature.

A new constitutive model for HCP metals

C.Y. Gao [a, b], L.C. Zhang [b,*], H.X. Yan [a]

[a] *Department of Mechanics, Zhejiang University, Hangzhou, 310027, China*

[b] *School of Mechanical and Manufacturing Engineering, The University of New South Wales, NSW 2052, Australia*

Abstract

This paper develops a new constitutive model for HCP metals subjected to high strain, high strain rate and high temperature based on the theory of thermally activated dislocation motion in crystal materials. The constitutive parameters of the material are determined by a new efficient method composed of a global genetic algorithm and a local penalty-function algorithm, which guarantees that the constitutive parameters are a globally optimal solution in their theoretically allowed ranges. The application of the model to Ti6Al4V alloy shows that in the high strain rate regime, the model prediction is much more accurate than those by the Johnson-Cook and Zerilli-Armstrong models.

Keywords: Constitutive modelling; plastic deformation; dislocation; high temperature; high strain rate; Ti6Al4V

[*] *Corresponding author. Tel.: +61 2 9385 6078; fax: +61 2 9385 7316.*
E-mail addresses: Liangchi.Zhang@unsw.edu.au

1. Introduction

An accurate description of the dynamic response of materials and structures under impact loading coupled with high strain and high temperature is important to many engineering fields. To reflect such plastic deformation behavior correctly, a reliable constitutive relation is necessary. In general, the dynamic yield stress of a material with a large plastic deformation and at high strain rates can be described by a function of state variables related to deformation history. Over the past decades, the investigation into the rate-dependent constitutive models has been extensive, among which the Johnson-Cook (J-C) equation based on the conventional phenomenological theory is one of the most widely used [1], because this model can successfully illustrate many experimental results and is convenient to use. However, it has also been reported that the J-C model does not function particularly when a material is subjected to a very high strain rate, such as under high speed machining [2]. This is because the dynamic behavior of a material at high strain rates is closely related to the material's microstructure evolution during plastic deformation, which is not taken into account in the conventional phenomenological modeling.

Zerilli and Armstrong proposed a constitutive relation with the aid of a thermal activation analysis [3]. They found that the dislocation mechanisms in metals of different crystalline structures vary. For face-centered cubic (FCC) metals, dislocations must traverse the barriers of forest dislocations, and the thermal activation area decreases with plastic strain due to the increase of dislocation density. Nevertheless, for body-centered cubic (BCC) metals, dislocations must overcome Peierls-Nabarro barriers (i.e., Peierls internal stress), and thus the

thermal activation area is not related to strain. Because of the above difference, Zerilli and Armstrong proposed different constitutive relations for FCC and BCC metals. Based on the same dislocation theory, Nemat-Nasser et al. introduced a more general model applicable to both FCC and BCC metals [4, 5], and determined the constitutive parameters of some typical metals on the basis of their improved Hopkinson pressure bar tests. Gao and Zhang proposed a dislocation-mechanics-based constitutive model to describe the dynamic plasticity of FCC metals [6], in which the microstructure evolution of crystalline materials is accommodated based on the concept of mechanical threshold stress (MTS, the flow stress at 0 K) established by Kocks in [7]. The application of the Gao-Zhang (G-Z) model to OFHC copper showed that it is simple to apply and gives a better prediction of the flow stress than the other models.

To date, studies in the field of constitutive modeling has been mainly on FCC and BCC metals due to their simple crystalline structures. Little has been done on the hexagonal close-packed (HCP) metals, particularly alloys of a more complicated crystalline structure, such as Ti6Al4V titanium alloy. Nemat-Nasser et al. proposed a constitutive model for Ti6A14V alloy by generalizing their model of OFHC copper [8]. Zerilli and Armstrong proposed a constitutive model for HCP metals (Z-A model) based on an argument that HCP metals have partial structural characteristics of BCC and FCC metals [9]. Khan et al. compared their modified Khan-Huang-Liang (KHL) model with the J-C model [10]. The conventional form of the J-C model for Ti6Al4V at high temperature was improved by introducing a temperature function to account for a drop in the flow stress due to dynamic recrystallization [11]. On the other hand, the plastic deformation mechanism of Ti6Al4V

alloy was experimentally studied too. Follansbee and Gray pointed out that sliding is the dominant plastic deformation mechanism in Ti6Al4V at relatively low strain rates, and the phenomenon of deformation twinning is prone to occur at high strain rates [12]. Lee and Chen carried out an impact test on Ti6Al4V and found that with the increase of strain rates, the thermal activation volume decreases and as such the sensitivity of the flow stress to the strain rate increases [13]. Lee and Lin [14] studied the temperature sensitivity of the flow stress of Ti6Al4V during high temperature deformation and fracture. Briottet et al. [15] observed the instability phenomenon of plastic deformation of Ti6Al4V under tension. Poletti et al. [16] studied the hot deformation of Ti6Al4V under compression, in which the local deformation parameters were correlated with the microstructural characteristics though not at high strain rates.

This paper will develop a new constitutive model for HCP metals, based on the theory of thermal activation mechanism of dislocation motion. An efficient method for determining the global optimal solution of material parameters will also be established.

2. Constitutive modeling of HCP metals

It has been established that plastic deformation of metals at high strain rates is basically a process of dislocation motion and accumulation under the rate-controlled deformation mechanism. Although the mechanism of HCP metals has not been clearly described by the conventional thermal activation theory for their complicated crystalline structure, it is true that the HCP structure owns partially the characteristics of both FCC and BCC structures. It

is therefore believed that the constitutive behavior of HCP metals may be reflected by a combination of those of the FCC and BCC metals.

For FCC metals, the barriers can be generally divided into short-range and long-range ones, where the former should be overcome by thermal activation while the latter are independent of the temperature (i.e. athermal). The short-range barriers may include forest dislocations (i.e., the intersection of dislocation forests, which is the principal mechanism in FCC metals), Peierls stress (i.e., the overcoming of Peierls-Nabarro barriers, which is the principal mechanism in BCC metals), point defects (e.g., vacancies and self-interstitials), alloy elements, solute atoms (interstitials and substitutionals), impurities, deposits and so on. The long-range barriers include grain boundaries, far-field dislocation forests and other microstructural elements with far-field influence. Therefore, the flow stress of the materials, which is essentially defined by the material resistance to dislocation motion, can be correspondingly decomposed into

$$\sigma = \sigma_a + \sigma_{th} \tag{1}$$

where σ is flow stress, σ_a is the athermal component of flow stress reflecting the effect of the long-range barriers, σ_{th} is the thermal component of flow stress reflecting the effect of the short-range barriers closely related with the thermal activation. For FCC metals, we have obtained the following constitutive relation [6]:

$$\sigma = \sigma_G + k_S d^{-1/2} + \hat{Y}\varepsilon^{n_1} \exp[\alpha T \ln(\dot{\varepsilon}/\dot{\varepsilon}_{s0})] \cdot \{1 - [-\beta T \ln(\dot{\varepsilon}/\dot{\varepsilon}_0)]^{1/q}\}^{1/p} \quad (2)$$

where ε (shear plastic strain), $\dot{\varepsilon}$ (shear plastic strain rate) and T (absolute temperature) are three state variables; $\hat{Y}$ is reference thermal stress; n_1 is the strain hardening exponent; $\dot{\varepsilon}_0$ is a reference strain rate; $\dot{\varepsilon}_{s0}$ corresponds to the saturated value of $\dot{\varepsilon}_0$; p and q are a pair of parameters representing the shape of crystal potential barrier; $\alpha = k/(a_0 \mu b^3)$ and $\beta = k/(g_0 \mu b^3)$ in which k is the Boltzmann constant, g_0 is nominal activation energy, a_0 is equivalent to its saturated value, μ is the shear modulus of material, and b is Burgers vector. $(\sigma_G + k_S d^{-1/2})$ is the athermal part of the flow stress, in which σ_G is the stress due to initial defects or impurities, d is the diameter of the grain and k_S is the slope coefficient. The term $k_S d^{-1/2}$ stands for the effect of grain size on flow stress which follows the classic form of the Hall-Petch relationship [17].

For BCC metals, the mechanical threshold stress, $\hat{\sigma}$, can also be similarly decomposed into

$$\hat{\sigma} = \hat{\sigma}_a + \hat{\sigma}_{th} \quad (3)$$

As there is no thermal activation energy at 0 K, the height of the short-range barriers is maximal. When temperature increases, the height will fall due to the increase of the atom vibration amplitude activated by the thermal energy, which helps a dislocation to overcome the barriers. Thus, the thermal stress will decrease while the athermal stress remains unchanged. If the MTS is regarded as a reference stress that characterizes the structure and its

evolution of a material, the flow stress can be expressed as

$$\sigma = \sigma_a + \sigma_{th} = \hat{\sigma}_a + f(\dot{\varepsilon}, T) \cdot \hat{\sigma}_{th} \tag{4}$$

where $f(\dot{\varepsilon}, T)$ is the influencing factor (<1), representing the strain rate and temperature effects. Hence, $\hat{\sigma}_a$, f and $\hat{\sigma}_{th}$ are the three key internal state variables to be determined, as detailed below.

(a) *Determination of* $\hat{\sigma}_a$

It is known that there exists an important difference between BCC and FCC metals in the mechanism of dislocation motion, i.e., the thermal activation area is closely related with strain for FCC metals, but it is not the case for BCC metals. Hence, the dynamic yield stress of FCC metals is determined mainly by strain hardening, but that of BCC metals is mainly determined by strain rate hardening and temperature softening. In other words, the strain hardening is coupled with the thermal stress for FCC metals, but not for BCC metals and belongs to the athermal stress then. The separated plastic strain-hardening contribution to the flow stress in BCC metals may be evaluated from an assumed power law dependence on strain [3], which has been verified by the experimental data obtained at sufficiently high temperatures (where the flow stress is essentially temperature-independent) [5], that is

$$\hat{\sigma}_a = \sigma_G + \sigma_S + K\varepsilon^n \tag{5}$$

where K is strain hardening coefficient and n is strain hardening exponent. σ_S ($=k_S d^{-1/2}$) is the grain-size stress induced by 'size effect', which can be regarded as a constant for a given material if there is no physical change (e.g. twinning) to alter the average grain size during plastic deformation. However, deformation twinning always takes place in the plastic deformation of BCC and HCP metals at high strain rates. Twinning subdivides the grains and therefore increases the barriers to slip and the work-hardening rate, and has a much lower sensitivity to strain rate and temperature. So the contribution of twinning to flow stress should also be incorporated into the athermal stress without changing the expression of the thermal stress. Meyers et al [18] pointed out that in most cases for FCC, BCC and HCP metals, the grain-size stress with twinning still obeys a Hall–Petch relationship, but with a slope k_T that is higher than the slope k_S for slip. That is to say, $\sigma_S = k_T d^{-1/2}$ ($k_T > k_S$). This larger grain size dependence of the twinning stress compared with the slip stress is a very unique characteristic of twinning, as pointed out by Armstrong and Worthington [19].

In reality, the H–P relationship has been experimentally verified to be also applicable to the relationship of strength and twin spacing (the mean spacing between adjacent twin boundaries) [20, 21]. Lu et al presented an analogous strengthening mechanism of twin boundary (TB) versus the strengthening mechanism of grain boundary (GB) in nanocrystalline (nc) metals by their experiments too [22, 23]. Klepaczko concluded that the effect of the twin spacing (λ) on the internal stress in polycrystalline metals and alloys follows the same relationship as that of the effect of the grain size (d) [24]. Based on this, the stress component due to the size effect can be expressed as

$$\sigma_S = k_{\mathrm{d}} d^{-1/2} + k_\lambda \lambda^{-1/2} \tag{6}$$

where k_d and k_λ are slope coefficients respectively.

Furthermore, the H-P relationship of the reciprocal of activation volume and the grain size has been observed. This size dependence was rationalized by combining the dislocation pile-up model and the thermal activation analysis of plastic flow rate. Considering the similar role of TB and GB (they are both effective in strengthening the material by blocking dislocation motion), there is a generalized H-P relationship for the reciprocal of activation volume [21]

$$V^{-1} - V_0^{-1} = k_{\mathrm{d}} d^{-1/2} + k_\lambda \lambda^{-1/2} \tag{7}$$

where V is activation volume and V_0 is the activation volume associated with the dislocation mechanism within the grains and twins. $k_{\mathrm{d}} = k_{\mathrm{d}}(V_{GB})$ and $k_\lambda = k_\lambda(V_{TB})$ where V_{GB} and V_{TB} are the activation volumes associated with the GB- and TB-mediated mechanism, respectively. Since $V \sim lb^2$ and $l^{-1} \sim \rho^{1/2}$ where l is the mean distance between forest dislocations, we have

$$(V^{-1} - V_0^{-1}) \sim \sqrt{(\rho - \rho_0)} \tag{8}$$

Among many reasonable evolution equation of dislocation density with strain, the most used is the simple but more realistic one proposed by Klepaczko [25]. By using this evolution equation, we obtained $\rho = \rho(\varepsilon)$ and then there is $\sigma_S = \sigma_S(\varepsilon)$. It was found that the functional curve of $\sigma_S \sim \varepsilon$ is almost the same as that of the power-law function. Considering that in the practical application of the physical constitutive model, the constitutive parameters are always determined as a whole by fitting the experimental data, the

homologous terms can be merged into one because the difference of this simplification can be mostly eliminated during the numerical fitting of parameters. As such, we can readily incorporate $\sigma_S(\varepsilon)$ into the power-law function $K\varepsilon^n$, and hence, the athermal stress can be simplified to

$$\hat{\sigma}_a = \sigma_G + \overline{K}\varepsilon^{\bar{n}} \tag{9}$$

In so doing, Eq. (9) becomes a unified expression of the athermal stress. The above analysis indicates that whether there appears twinning or not, Eq. (9) remains the same provided that the parameters are determined by corresponding data. Besides, compared with the thermal component of the flow stress, the size effect of twinning is relatively limited unless the twin spacing approaches to several hundred nanometers or less.

(b) *Determination of* f

The dislocation motion in plastic deformation of metals is driven by the flow stress caused by the external force of dynamic loading. Orowan proposed the relation between the plastic strain rate and the average dislocation velocity [26]. Gilman et al. obtained the relation of dislocation velocity and thermal activation energy [27]. These two relations are linked by the well-known Arrhenius expression:

$$\dot{\varepsilon} = \dot{\varepsilon}_0 \exp(-\Delta G(\sigma)/kT) \tag{10}$$

where the reference strain rate $\dot{\varepsilon}_0 = m'b\rho_m v_0$ (m' is the Schmidt factor, b is the Burgers vector representing the excursion induced by dislocation, ρ_m is the moving dislocation

density, and v_0 is the limit dislocation velocity). ΔG is the free energy of thermal activation (also called Gibbs free energy), which is a function of stress related to the barrier shape (e.g., rectangular, square, triangular, parabolic and exponential). Kocks and Ashby [28] proposed the following generalized equation with two parameters to fit any shapes:

$$\Delta G = G_0\left(1-(\sigma_{th}/\hat{\sigma}_{th})^p\right)^q \tag{11}$$

where G_0 $(=g_0\mu b^3)$ is the reference free energy at 0 K. Combining Eqs. (10) and (11) and considering Eq. (4), we can obtain

$$f(\dot{\varepsilon},T) = \{1-[-(kT/G_0)\ln(\dot{\varepsilon}/\dot{\varepsilon}_0)]^{1/q}\}^{1/p} \tag{12}$$

Thus, the influencing factor f is determined at the current constant structure.

(c) *Determination of* $\hat{\sigma}_{th}$

The strain hardening rate decreases with strain and approaches saturation due to dynamic recovery. Kocks [29] proposed an expression to describe the saturation threshold stress $\hat{\sigma}_s = \hat{\sigma}_s(\dot{\varepsilon},T)$ for FCC metals where dynamic recovery occurs by cross-slip, i.e.,

$$\ln(\dot{\varepsilon}/\dot{\varepsilon}_{s0}) = (a_0\mu b^3/kT)\ln(\hat{\sigma}_s/\hat{\sigma}_{s0}) \tag{13}$$

where $\dot{\varepsilon}_{s0}$ and $\hat{\sigma}_{s0}$ are the reference constants respectively. Cross-slip is important to the recovery processes in both FCC and BCC metals [30], and is observed from the initial stages of deformation in BCC single crystals. It seems to be a general feature of plastic deformation

in many BCC metals that the mobility of dislocations is limited by cross-slip processes. The mobile dislocations due to slip rates get annihilated with immobile dislocations either through cross-slip of screws or through annihilation of edges of opposite signs [31]. Hence, cross-slip as a thermally activated process also plays a crucial role in the dynamic recovery mechanism of BCC metals. Since the expression of saturation stress is actually obtained from the calculations by Schoeck and Seeger [32] of the stress dependence of the activation energy for cross-slip, it is reasonable to use it for both FCC and BCC metals considering their similar recovery mechanism, as what has been done by Kocks in the deformation of 304L stainless steel besides aluminum and copper [7] – a valid precedent of application to BCC metals. Hence, using Eq. (13) for BCC metals, the thermal component of saturation threshold stress, $\hat{\sigma}_{th,s}$, can be obtained approximately with $\hat{\sigma}_s / \hat{\sigma}_{s0} \cong \hat{\sigma}_{th,s} / \hat{\sigma}_{th,s0}$ (here $\hat{\sigma}_{th,s0}$ is also a reference constant):

$$\hat{\sigma}_{th,s} = \hat{\sigma}_{th,s0} \exp[(kT / a_0 \mu b^3) \ln(\dot{\varepsilon} / \dot{\varepsilon}_{s0})] \tag{14}$$

Furthermore, because the thermal stress in BCC metals is independent of strain, the thermal component of MTS should be the same as its saturated value, i.e., $\hat{\sigma}_{th} = \hat{\sigma}_{th,s}$. By letting $\hat{\sigma}_{th0} = \hat{\sigma}_{th,s0}$, we get

$$\hat{\sigma}_{th} = \hat{\sigma}_{th0} \exp[(kT / a_0 \mu b^3) \ln(\dot{\varepsilon} / \dot{\varepsilon}_{s0})] \tag{15}$$

It is noticed that the above constitutive expression has the same form as that of the thermal stress in the classic Z-A relation. Such a consistency manifests, in a sense, the rationality of

applying Eq. (13) in BCC metals.

Now, substituting Eqs. (5), (12) and (15) into Eq. (4), we obtain the following relation:

$$\sigma = \sigma_G + \overline{K}\varepsilon^{\bar{n}} + \hat{\sigma}_{th0}\exp\left[\alpha T \ln\left(\dot{\varepsilon}/\dot{\varepsilon}_{s0}\right)\right]\cdot\left\{1-\left[-\beta T \ln\left(\dot{\varepsilon}/\dot{\varepsilon}_0\right)\right]^{1/q}\right\}^{1/p} \tag{16}$$

where α and β are as defined in Eq. (2).

With all the above available, we can now establish the constitutive model for HCP metals.

The flow stress of HCP metals can be homo-plastically decomposed as the sum of the athermal stress and the thermal stress. The athermal stress is basically independent of strain rate and temperature but certainly has strain dependence reflecting the structural evolution. Although the athermal stress of FCC metals is assumed as a constant in [3, 6, 7], its strain dependence is found in [4] with the same form as BCC metals. So, the expression of the athermal stress of BCC metals can be regarded as a general form which can be used here for HCP metals:

$$\sigma_{ath} = \sigma_G + \overline{K}\varepsilon^{\bar{n}} \tag{17}$$

Considering that HCP metals own partial structural characteristics of both BCC and FCC metals, Zerilli and Armstrong introduced both Peierls stress type interactions (predominant in

BCC) and intersection-of-forest-dislocation type interactions (predominant in FCC) into a single equation by using the principle of linear superposition, in order to describe the intermediate behavior of HCP metals and certain high-strength alloy steels [9]. By this means, the thermal stress of HCP metals can be written as the following combined form:

$$\begin{aligned}\sigma_{th} = {} & l_1 \cdot \hat{Y}\varepsilon^{n_1} \exp[\alpha_1 T \ln(\dot{\varepsilon}/\dot{\varepsilon}_{s0,1})] \cdot \{1-[-\beta_1 T \ln(\dot{\varepsilon}/\dot{\varepsilon}_{0,1})]^{1/q_1}\}^{1/p_1} \\ & + l_2 \cdot \hat{\sigma}_{th0} \exp[\alpha_2 T \ln(\dot{\varepsilon}/\dot{\varepsilon}_{s0,2})] \cdot \{1-[-\beta_2 T \ln(\dot{\varepsilon}/\dot{\varepsilon}_{0,2})]^{1/q_2}\}^{1/p_2}\end{aligned} \tag{18}$$

where l_1 and l_2 are linear constant coefficients, reflecting the proportion of FCC and BCC structural characteristics in a HCP structure. The constitutive expression in Eq. (18) is still not very practical in its application, because it contains 15 parameters to be determined. Since the parameters of a physical constitutive model are often determined by numerical fitting based on relevant experimental data, too many parameters will make the calculation process extremely nonlinear and difficult to get convergence. To guarantee that convergence in the parameter determination of our new constitutive model, let us further carry out a simplification for Eq. (18). We note that there are similar functional forms in the first and the second terms of this equation, which have the same physical meaning and may be merged. Based on this consideration, Eq. (18) can be rewritten as

$$\sigma_{th} = (\hat{\sigma}_{th0} + \hat{Y}\varepsilon^{n_1}) \exp[\alpha T \ln(\dot{\varepsilon}/\dot{\varepsilon}_{s0})] \cdot \{1-[-\beta T \ln(\dot{\varepsilon}/\dot{\varepsilon}_0)]^{1/q}\}^{1/p} \tag{19}$$

In this way, the number of the thermal stress parameters is reduced from 15 in Eq. (18) to 9 in Eq. (19), which will effectively enhance the convergence stability in determining the

parameters. Now, by combining Eqs. (17) and (19), we obtain the following constitutive model for HCP metals, which is easy to use,

$$\sigma = \sigma_G + \overline{K}\varepsilon^{\bar{n}} + (\hat{\sigma}_{th0} + \hat{Y}\varepsilon^{n_1})\exp[\alpha T \ln(\dot{\varepsilon}/\dot{\varepsilon}_{s0})]\cdot\{1-[-\beta T \ln(\dot{\varepsilon}/\dot{\varepsilon}_0)]^{1/q}\}^{1/p} \tag{20}$$

The constitutive parameters to determine include $\sigma_G, \overline{K}, \bar{n}, \ \hat{\sigma}_{th0}, \hat{Y}, n_1, \alpha, \beta, \dot{\varepsilon}_{s0}, \dot{\varepsilon}_0, p, q$.

3. Some remarks

3.1 Adiabatic deformation

The new constitutive equation, Eq. (20), is applicable not only to an isothermal deformation process (mainly at low strain rates), but also to an adiabatic deformation process (mainly at high strain rates). If a localized adiabatic shear phenomenon happens at high strain rates, the majority of the plastic work will be converted to the internal dissipation heat in materials, and will cause a rapid increase of local temperature. The increased temperature can be calculated by

$$T = T_0 + \frac{\eta}{\rho_M c_p}\int_0^{\varepsilon}\sigma\, d\varepsilon \tag{21}$$

where T_0 is the initial temperature, ρ_M is the material's density, c_p is the material's specific heat at constant pressure, and η is the converting efficiency from plastic work to heat (also called the Taylor-Quinney empirical constant, ranging generally between 0.9 and 1.0). Of course, in an adiabatic calculation of flow stress by Eq. (20), the state variable of

temperature should be updated continuously at each strain increment.

3.2 Dynamic strain aging and recrystallization

Anurag and Guo [33] found in their tests on 6061-T6 aluminum that the flow stress is least sensitive to temperature within a certain range, and the flow stress recovers its previous dependence on temperature if the temperature is beyond the certain range. They attributed such phenomenon to the dynamic strain aging due to the mutual interaction of dislocations and solute atoms. Meyers et al. found in their tests on OFHC copper that there is a drop in the flow stress when the temperature reaches a certain value, which is related to the dynamic recrystallization and phase transition [34]. In both of the above two cases, an empirical temperature function is used to correct the flow stress when temperature is higher than a certain turning point. However, there does not seem to have such phenomenon in the flow stress variation of Ti6Al4V titanium alloy [8, 33]. Nemat-Nasser concluded that their constitutive model of Ti6Al4V predicts experimental data very well without considering dynamic strain aging. It is therefore rational that our HCP constitutive model does not need to include the dynamic strain aging and dynamic recrystallization.

3.3 Critical temperature and deformation twinning

During plastic deformation, the thermal component of flow stress in materials decreases with the temperature rise and eventually disappears at a critical temperature $T^{cr} = [-(k/G_0)\ln(\dot{\varepsilon}/\dot{\varepsilon}_0)]^{-1}$ [5]. Hence, beyond T^{cr}, the thermal component of flow stress should be removed from Eq. (20).

Although many HCP metals undergo deformation twinning, Tirry et al. [35] pointed out that the fraction of deformation twins in Ti6Al4V is very low, indicating that twinning is not a major deformation mechanism for Ti6Al4V alloy, and dislocation motion is dominating through planar slips with negligible amounts of twin deformation. The result is consistent with the study by Follansbee and Gray [12], where the authors found deformation twins only at very high strain rate experiments. The behavior is attributed to a reduced dislocation mobility requiring high stresses for deformation, resulting in development of deformation twinning at very high strain rate and low temperatures.

4. Determination of constitutive parameters

4.1 Optimization algorithm

The identification of the constitutive parameters is to obtain a group of optimal parameter values to make the theoretical prediction a best fit to experimental data. In the literature, the process is to fit each parameter individually. In so doing, the parameters determined are not optimal as a whole and each single evaluation is susceptible to random discrete errors of experimental data. Here, we will use a multi-variable nonlinear optimization method to obtain the optimal parameters as a whole.

The objective function for the parameter optimization is defined as the sum of the square of the difference between the flow stress prediction and experimental data at each sample point, i.e.,

$$\min\ f(\mathbf{x}), \quad f(\mathbf{x}) = \sum_{i=1}^{N} (Y_i(\mathbf{x}) - Y_i^*)^2 \tag{22}$$

where $\mathbf{x} = [x_1, \cdots, x_m]\,(m = 7)$, Y_i is the calculated flow stress at the ith point, Y_i^* is the corresponding experimental data, and N is the number of the sample points. The constitutive parameters are regarded as a group of independent variables of the function. The optimization is to obtain a group of variables making the function minimum.

The optimization methods can be divided into two types. One is determinate method based on a gradient search technique, which converges quickly but depends strongly on the initial values of variables, resulting in the risk of not obtaining a globally optimal solution. The other is the indeterminate method based on a random search technique, which is insensitive to the initial values of variables, but its calculating scale is huge and is not determinate to obtain the global optimal solution finally.

To overcome these problems, we will combine a local algorithm (LA) and a global genetic algorithm (GA), by first carrying out a GA with a moderate calculating scale to obtain a group of preliminary optimized results, and then using a LA with these preliminarily global optimized results as the initial values of the variables to obtain the final optimized results. A Matlab program has been written to carry out the above optimization procedure, demonstrated by the flowchart shown in Fig. 1 where e% is an allowed error threshold value. Moreover, to guarantee the precision of the result of a local optimization, it is necessary to

understand the theoretical range of each parameter in the constitutive model. Such range limits are treated as inequality constraints in the interior-point penalty function method which is adopted as our LA here [36]. The range limits for Ti6Al4V will be discussed in detail below.

4.2 Constitutive parameters for Ti6A14V

Ti6A14V titanium alloy is of HCP structure and has been widely used in many engineering fields, such as in aerospace engineering, due to its attractive specific strength and corrosion resistance. A deep understanding of the material's thermo-mechanical response during its plastic deformation at high strain rates and high temperatures is of primary importance. We therefore take Ti6A14V as a typical HCP metal to demonstrate the applicability of our new constitutive model. The constitutive parameters of Ti6A14V are determined as follows:

(a) σ_G, $\overline{K}$ *and* $\bar{n}$

First, we will determine the parameters of the athermal stress which is separated with the thermal stress and has a simple functional form. The experimental data used for the athermal stress are obtained at sufficiently high temperatures where the flow stress is essentially independent of temperature. So, in order to get accurate values of the athermal stress, we adopted a stress-strain curve of Ti6Al4V at strain rate of 3,700/s and at temperature greater than 1,000 K [8]. The three parameters determined are

$$\sigma_G = 60\,MPa \ , \ \overline{K} = 660.4 \ , \ \bar{n} = 0.053$$

(b) $\dot{\varepsilon}_{s0}$ *and* $\dot{\varepsilon}_0$

The two reference strain rates, $\dot{\varepsilon}_0$ and $\dot{\varepsilon}_{s0}$, can be evaluated before the optimal calculation of the other parameters, because the influence of the two is small (they are in the logarithmic functions) relative to that of α and β. Since $\dot{\varepsilon}_{s0}$ and $\dot{\varepsilon}_0$ are dependent on α and β respectively, the errors in evaluating them can be offset in the fitting of α and β. In so doing, we not only avoid the scattering problem in the literature [8, 9, 33], but also enhance the robustness of the nonlinear optimization for determining the rest of the parameters. According to [8], the average reference strain rate is $\dot{\varepsilon}_0 = 3\times10^9 s^{-1}$ at $\varepsilon = 0.25$ and $T = 598K$. Although the direct evaluation of the saturated reference strain rate is unavailable, we can designate $\dot{\varepsilon}_{s0} = 1.0\times10^{11} s^{-1}$ by considering that it is generally greater than $\dot{\varepsilon}_0$ by two orders.

With these parameters ready, the remaining seven parameters in the thermal stress to determine are $\hat{\sigma}_{th0}, \hat{Y}, n_1, \alpha, \beta, p, q$. Firstly, the theoretical ranges of them need to be discussed seriatim:

(c) Ranges of $\hat{\sigma}_{th0}$ *and* $\hat{Y}$

If $\hat{\sigma}_{th0}$=1560 MPa in the literature is regarded as its average value, its variation range can be set as [1000, 2000] MPa. $\hat{Y}$ is corresponding to a term related with temperature defined in [8]. Considering the actual varying range of [77, 998] K, we obtain the varying range of $\hat{Y}$ as [1500, 3500] MPa.

(d) Ranges of α *and* β

In the definition of $\beta = k/(g_0 \mu b^3)$, the Boltzmann constant $k = 1.3806505\times10^{-23}$ J/K, shear modulus $\mu = E/2(1+\upsilon) = 42GPa$ and Burgers vector $b = 3\times10^{-10}m$ have been known. The only unavailable constant is the nominal activation energy g_0. However, it is known [37] that g_0 is within the range of [0.2, 2] for medium strength of a single obstacle of barriers. Thus there is $\beta \in [6\times10^{-6}, 6\times10^{-5}]$. We can extend this range to $[1\times10^{-6}, 1\times10^{-4}]$ considering a wider range of g_0 outside the moderate obstacle strength. Because a_0 is of the same order as g_0, the theoretically allowed ranges of α and β are the same.

(e) Range of n_1

The thermal stress in most FCC metals is basically proportional to the square root of strain [12], so the value of n_1 for FCC metals is around 1/2. But in the constitutive model of Ti6Al4V [8], the value is set as 1.0. So, the maximum range of n_1 can be considered as [0, 1].

(f) Ranges of p *and* q

As we know, (p, q) is a pair of parameters representing the shape of crystal potential barrier. According to the physical nature of the barrier, there is $p \in (0, 1]$ and $q \in [1, 2]$ for single crystal structure [28]. Some typical cases of the (p, q) pair are: (2/3, 1) for a rectangular barrier, (1/2, 2) for a hyperbolic barrier and (1, 2) for a sinusoidal barrier. The other commonly used values of (2/3, 1), (2/3, 2), (3/4, 4/3) and (1, 1) all can be considered as the

transitional shape between the rectangle and the sinusoid. Though the range above is for single crystal structure, it is suitable for the mixed structure of HCP metals too because in our constitutive relation the related term of HCP metals is equivalent to the mathematical mean of the corresponding terms of FCC and BCC metals. Furthermore, it can be proved in simplified cases that there are $\min(p_1, p_2) \le p \le \max(p_1, p_2)$ and $\min(q_1, q_2) \le q \le \max(q_1, q_2)$.

With the parameter ranges above as the constraint condition of optimization, the combined GA and LA optimizing method was then carried out to obtain the optimal set of the constitutive parameters. The optimization was based on the experimental data of a group of stress-strain curves of Ti6A14V alloy measured by Nemat-Nasser et al. [8] at different temperatures and strain rates (i.e., [1,900s^{-1}, 77K], [1,900s^{-1}, 296K], [2,700s^{-1}, 598K] and [3,100s^{-1}, 798K]). The results have been listed in Table 1.

5. Results and discussion

In the following results, all the theoretical predictions of flow stress are of the adiabatic process and so the temperature indicated is initial temperature, except the case of quasi-static strain rate of 0.001 s^{-1}.

Figure 2 compares the flow stress predictions of our model with the experimental data which have been used to fit the constitutive parameters. It is a basic validation of our model to see if the model prediction can effectively comply with the varying tendency of experimental data. The comparison indicates that the model describes well the flow stress behavior of Ti6Al4V

alloy within a broad temperature range at high strain rates.

Figure 3 shows our model prediction of flow stress at 2,000 s^{-1}. The experiment data and the results of the J-C [38] and Z-A [9] models are also presented for comparison. It is clear that our model is good at this strain rate level for both room and high temperatures. The J-C model is good at 598 K but tends to the low side at room temperature when the strain exceeds 0.15. The Z-A model gives too high predictions within the whole strain range especially at high temperature, though it seems in accordance with some earlier experimental data [39] where the strain is only below 0.15 and the strain rate is relatively low. So it can be concluded that in the case of high temperature, the Z-A type model is unsuitable not only for FCC and BCC metals (as pointed out by Armstrong themselves in [3]) but also for HCP metals.

Figure 4 compares the flow stress predictability of different models at high strain rate of 6,000 s^{-1} (room temperature). It is obvious that our model is better than others at relatively high strain rates (average error less than 5%). The J-C model still tends to the low side more and more when the strain exceeds 0.15.

Figure 5 presents the different flow stress predictions under quasi-static loading of 0.001 s^{-1}. It seems that our new model does not predict well for the case of very low strain rates, though better than the Z-A model, further indicating that our model is best applicable to the case of high strain rates.

Figure 6 shows the dependence of flow stress on temperature at different strains and a given strain rate of 2000 s^{-1}. Our model predicts the experimental data [8] quite well. Based on the discussion of critical temperature in Section 2, we understand that the critical temperature is dependent on the strain rate. For the stain rate shown in Fig. 6, the critical temperature of Ti6Al4V is 1,172 K. It can be seen in this figure that when temperature approaches the critical value, the thermal stress decays very slowly and becomes nearly zero, at which only the invariable athermal stress in the flow stress remains finally. This result confirms that it is rational to decompose the flow stress into the athermal and thermal components at the beginning of the constitutive modeling.

In addition, it can be proved mathematically that the stress-temperature curve should be convex towards the coordinate origin under the physical condition of $p \in (0, 1]$ and $q \in [1, 2]$. However, Anurag and Guo [33] argued that the curve could be concave according to their experimental data. If they were correct, there would be $p > 1$ which would violate the physical meaning of the parameter. We carefully analyzed their experimental data and found that their stress-temperature curve is not truly concave. It may be described as three consecutive sections just before, in and after the temperature transition zone. As pointed out by Lee and Lin [14] with their own high-temperature experiments, the relationship in each section should be linear. Hence, the limit case of ($p = 1, q = 1$), corresponding to a whole linear relationship of stress and temperature, may approximately represent the multi-straight-line experimental curve of [33] and thus explain the exceptional situation reasonably.

To find more predictive capability of our model , the flow stress predictions of our model were compared in Fig. 7 with some other experimental data ----One is by Khan et al [38] and another is by Harding et al [40]. As shown in the figure, our model prediction of the former experimental data supports its applicability. There is a gap between the model prediction and the latter experimental measurement. This is understandable if we note that they adopted the thin-walled tubular specimens of Ti6Al4V alloy in their torsional or tensile impact tests which is different from the bar specimens in SHPB tests.

6. Conclusions

Based on the theory of thermally activated dislocation motion for the plastic deformation of crystal materials, we have developed a new, practical constitutive model for HCP metals. The material parameters of the constitutive model are determined by a new optimization method which is composed of the global genetic algorithm and a local penalty-function algorithm. The new method guarantees that the constitutive parameters determined are globally optimized in their theoretically allowed ranges. The application of the new model to the flow stress prediction of Ti6Al4V shows that compared with the widely used Johnson-Cook and Zerilli-Armstrong models, ours can describe more accurately the material's behavior in a broad range of strain, strain rate and temperature.

Acknowledgments

This research work is supported the Australian Research Council's Linkage-Project and by

the Project of the National Natural Science Foundation of China under Grant No. 50890174 and 50877070.

References

[1] G. Johnson, W. Cook, Eng. Fract. Mech. 21(1985) 31-48.

[2] J.A. Arsecularatne, L.C. Zhang, Key Eng. Mater. 274-276 (2004) 277-282.

[3] F.J. Zerilli, R.W. Armstrong, J. Appl. Phys. 61 (1987) 1816-1825.

[4] S. Nemat-Nasser, Y.L. Li, Acta Mater. 46 (1998) 565-577.

[5] S. Nemat-Nasser, J.B. Isaacs, Acta Mater. 45 (1997) 907-919.

[6] C.Y. Gao, L.C. Zhang, Mater. Sci. Eng. A 527 (2010) 3138-3143.

[7] P.S. Follansbee, U.F. Kocks, Acta Metall. 36 (1988) 81-93.

[8] S. Nemat-Nasser, W.G. Guo, V.F. Nesterenko, S.S. Infrakanti, Y.B. Gu, Mech. Mater. 33 (2001) 425-439.

[9] F.J. Zerilli, R.W. Armstrong, In: High Strain Rate Effects on Polymer, Metal and Ceramic Matrix Composites and Other Advanced Materials, ASME, New York, 1995, pp. 121–126.

[10] A.S. Khan, R. Kazmi, B. Farrokh, M. Zupan, Int. J. Plasticity 23 (2007) 1105-1125.

[11] S. Seo, O. Min, H. Yang, Int. J. Impact Eng. 31 (2005) 735-754.

[12] P.S. Follansbee, G.T.III. Gray, Metal. Trans. A 20 (1989) 863-874.

[13] W.S. Lee, T.H. Chen, H.C. Huang, J. Nuclear Mater. 402 (2010) 1-7.

[14] W.S. Lee, C.F. Lin, J. Mater. Process. Tech. 75 (1998) 127-36.

[15] L. Briottet, A. Ambard, D. Guichard, Model. Simul. Mater. Sci. Eng. 9 (2001) 259-277.

[16] C. Poletti, F. Warchomicka, H.P. Degischer, Mater. Sci. Eng. A 527 (2010) 1109-1116.

[17] R.J. Lederich, S.M.L. Sastry, J.E. O'Neal, B.B. Rath, Mater. Sci. Eng. A 33 (1978) 183-188

[18] M.A. Meyers, O. Vohringer, V.A. Lubarda, Acta mater. 49 (2001) 4025–4039.

[19] R.W. Armstrong, P.J. Worthington, In: Metallurgical Effects at High Strain Rates. Plenum Press, New York, 1973, 401–414.

[20] M.A. Meyers, K.K. Chawla, Mechanical behavior of materials. Prentice Hall, 1999.

[21] K. Konopka, J. Wyrzykowski, Mater. Proc. Tech. 64 (1997) 223.

[22]L. Lu, M. Dao, T. Zhu and J. Li, Scripta Materialia 60 (2009) 1062-1066.

[23] Y. F. Shen, L. Lu, Q. H. Lu, Z. H. Jin, K. Lu, Scripta Mater. 52 (2005) 989.

[24] J.R. Klepaczko, Nuclear Engineering and Design 127 (1991) 103-115.

[25] J.R. Klepaczko, A. Rouxel, C.Y. Chiem, Proc. Cong. Int. DYMAT 85 (Editions de Physique), 1985, C5-57.

[26] E. Orowan, Proc. Phys. Soc. 52 (1940) 8-22.

[27] W.G. Johnson, J.J. Gilman, J. Appl. Phys. 30 (1959) 129-144.

[28] U.F. Kocks, A.S. Argon, M.F. Ashby, In: Progress in Materials Science, Pergamon Press, 1975, 19, pp. 1-.

[29] U.F. Kocks, J. Eng Mater. Tech. 98 (1976) 76-.

[30] M. Rhee, H. Zbib, J. Hirth, H. Huang, T. Rubia, Model. Simulat. Mater. Sci. Eng. 6 (1998) 467–492.

[31] B. Peeters, M. Seefeldt, C. Teodosiu, S.R. Kalidindi, P. Van Houtte, E. Aernoudt, Acta Materialia 49 (2001) 1607-1619.

[32] G. Schoeck, A. Seeger, Defects in Crystalline Solids, Physical Society, London (1955).

[33] S. Anurag, Y.B. Guo, Int. J. Mech. Sci. 49 (2007) 909-918.

[34] M.A. Meyers, Dynamic Behavior of Materials. New York, John Wiley & Sons, Inc., 1994.

[35] W. Tirry, F. Coghe, S. Bouvier, M. Gasperini, L. Rabet, D. Schryvers, Mater. Sci. Eng. A 527 (2010) 4136-4145.

[36] R.H. Byrd, E.H. Mary, N. Jorge, J. Optimization 9 (1999) 877–900.

[37] H.J. Frost, M.F. Ashby, Deformation Mechanism Maps. Pergamon Press, Oxford, 1982.

[38] A.S. Khan, Y.S. Suh, R. Kazmi, Int. J. Plasticity 20 (2004) 2233-2248.

[39] K. Ogawa, T. Nojima, J. Soc. Mater. Sci. JPN 37 (1988) 41-.

[40] D.A.S. Macdougall, J. Harding, J Mech. Phys. Solids 47 (1999) 1157-1185.

List of Tables:

Table 1 Final optimized results for constitutive parameters of Ti6A14V

List of Figure Captions:

Fig. 1 Flowchart of the optimization procedure for constitutive parameter determination.

Fig. 2 Comparisons of flow stress prediction with experimental data of Ti6A14V at different strain rates and temperatures.

Fig. 3 Comparisons of flow stress predictions of different models with experimental data of Ti6A14V at 2,000 s^{-1} and indicated initial temperatures.

Fig. 4 Comparisons of different flow stress predictions with experimental data of TI6A14V at 6,000 s^{-1} and room temperatures.

Fig. 5 Comparisons of different flow stress predictions with experimental data of TI6A14V at 0.001 s^{-1} and room temperatures.

Fig. 6 Dependence of flow stress of Ti6Al4V on temperature at 2,000 s^{-1} and different strains.

Fig. 7 Comparisons of our model predictions with others' experimental data of TI6A14V alloy.

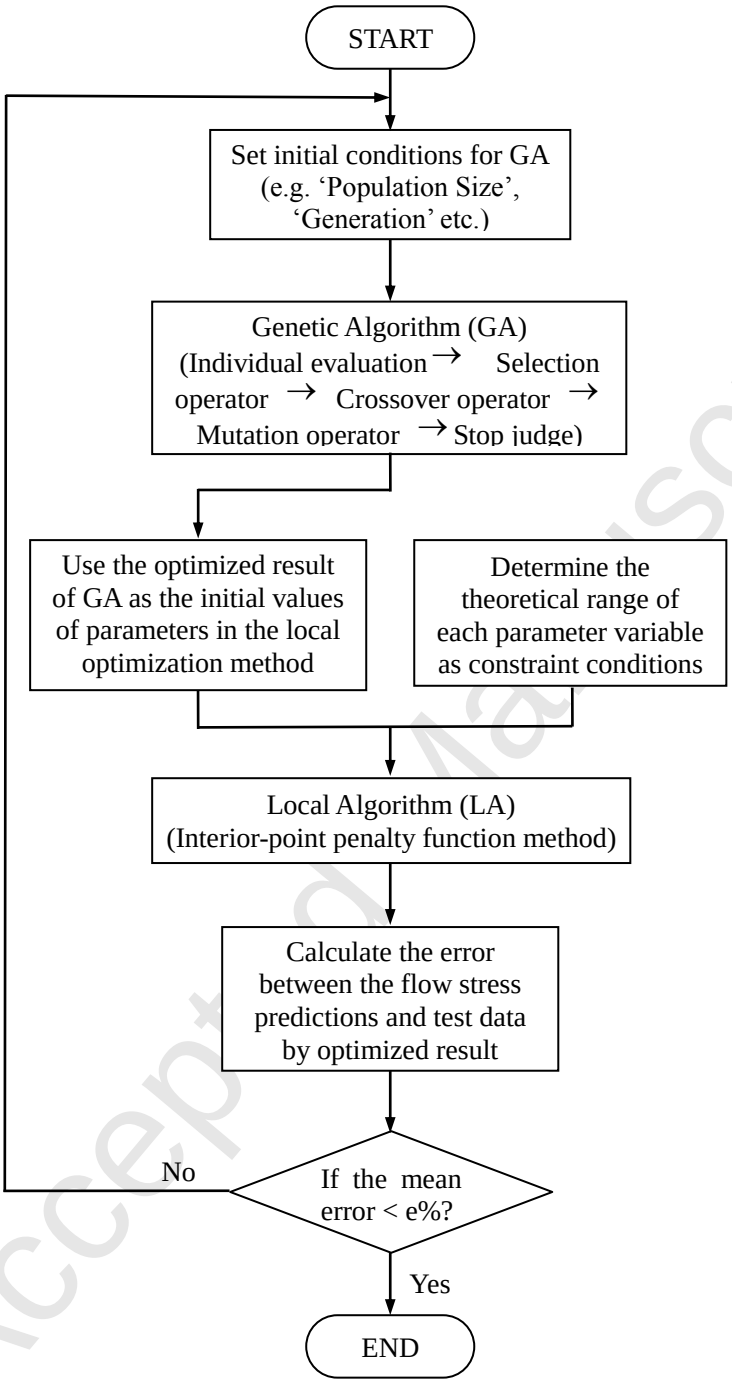

Fig. 1 Flowchart of the optimization procedure for the determination of constitutive parameters.

Figure(s)
Click here to download high resolution image

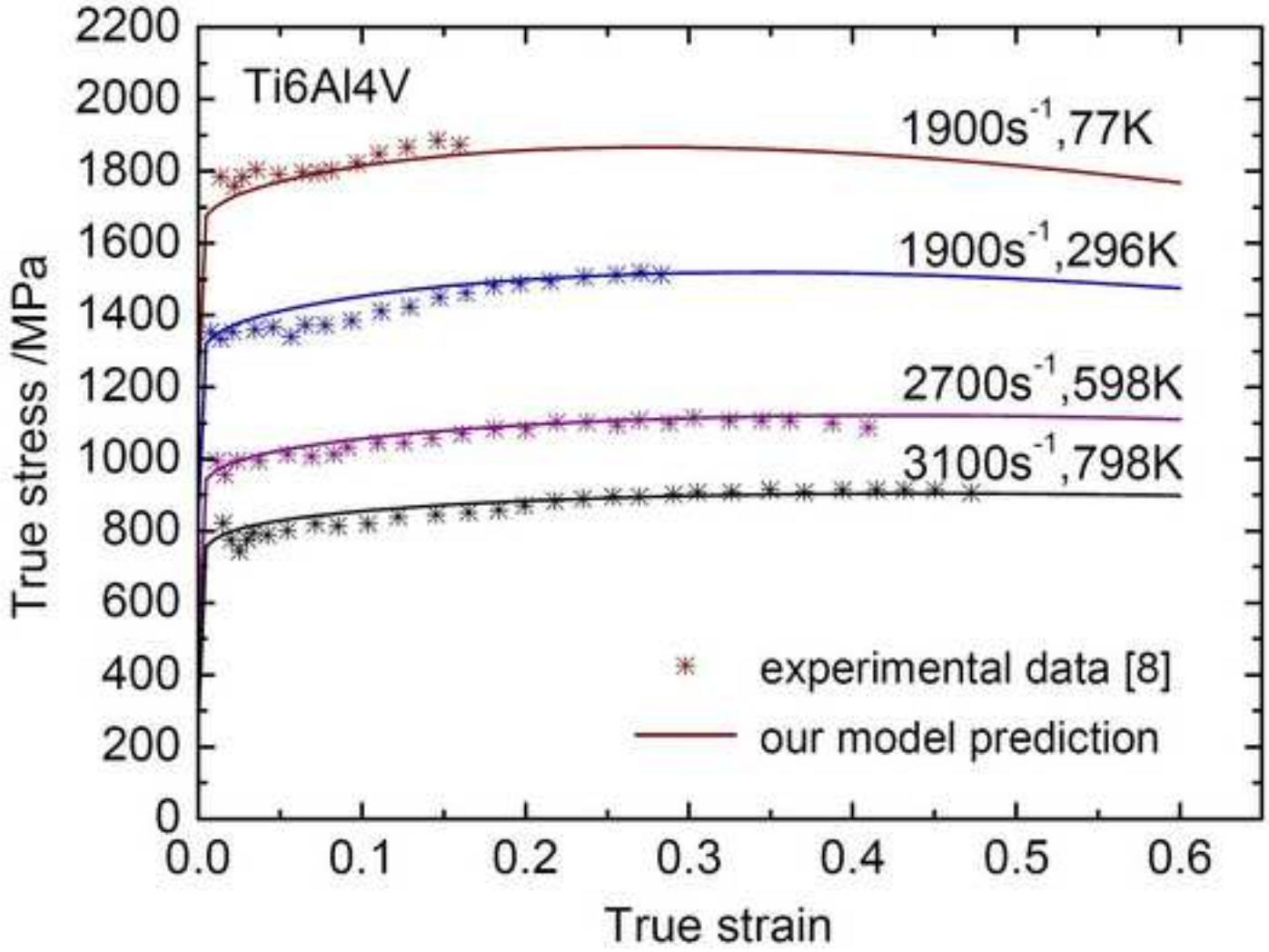

Fig. 2 Comparisons of flow stress prediction with experimental data of Ti6A14V at different strain rates and temperatures.

Figure(s)
Click here to download high resolution image

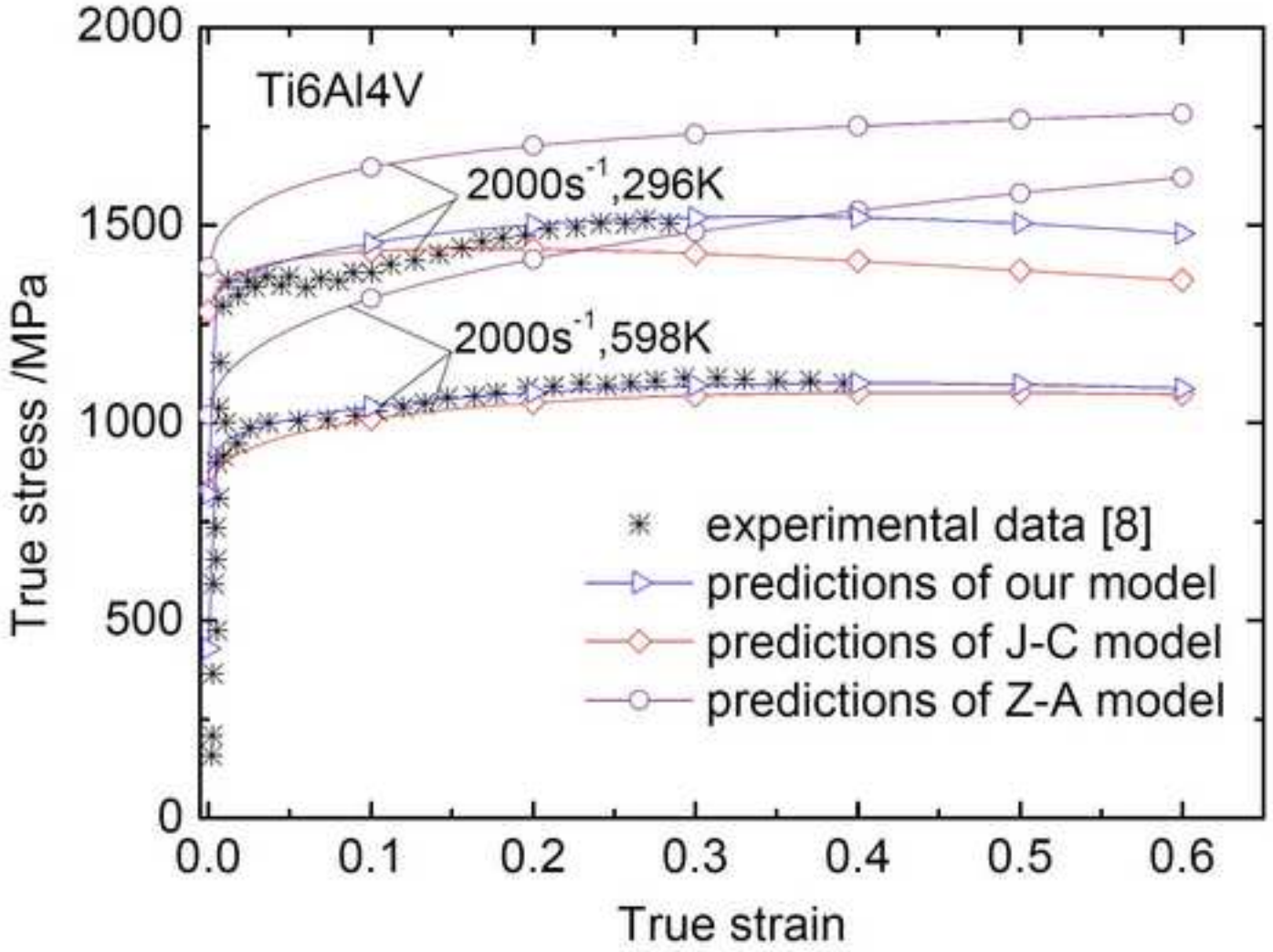

Fig. 3 Comparisons of flow stress predictions of different models with experimental data of Ti6A14V at 2000 s^{-1} and indicated temperatures.

Figure(s)
Click here to download high resolution image

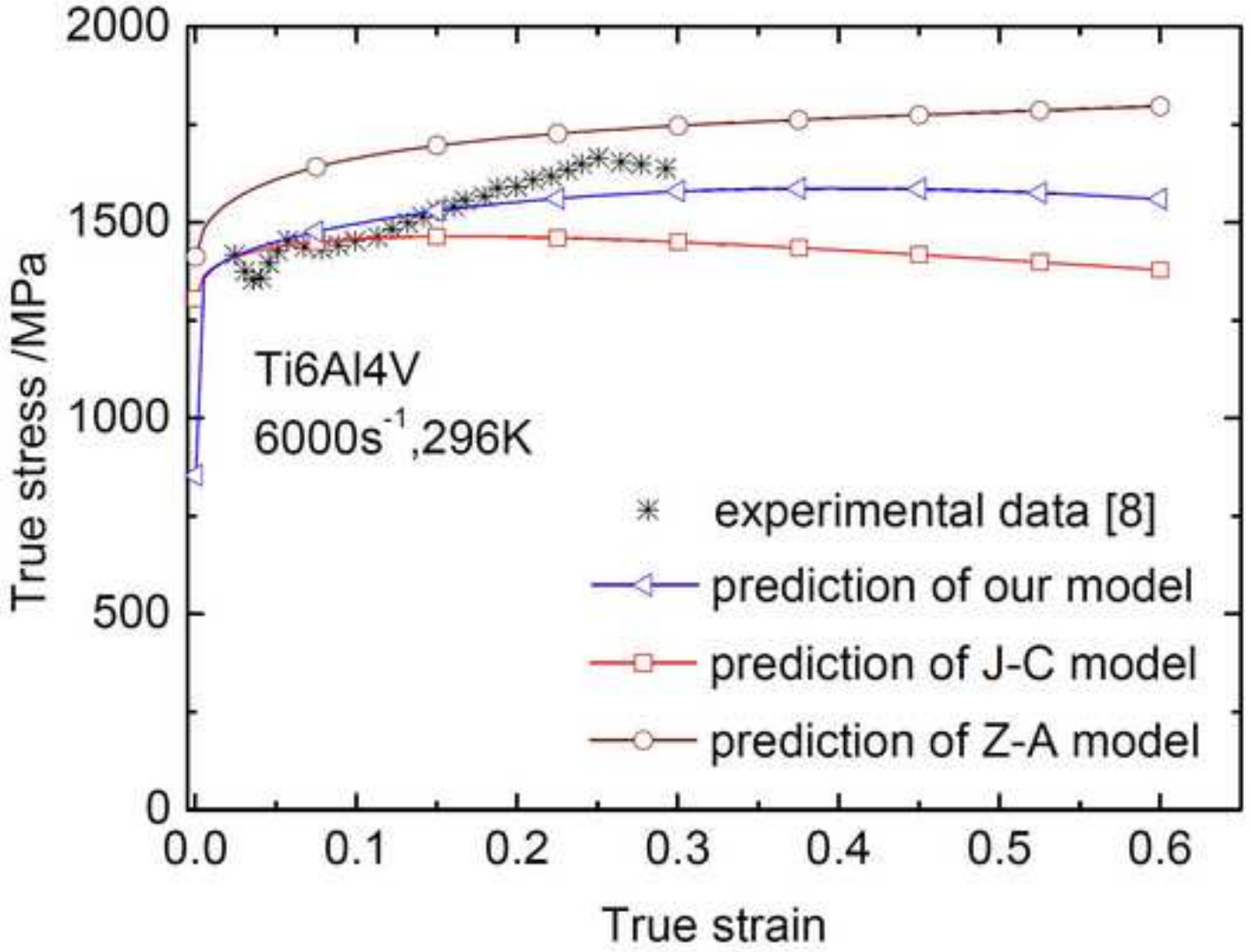

Fig. 4 Comparisons of different flow stress predictions with experimental data of TI6A14V at 6000 s^{-1} and room temperatures.

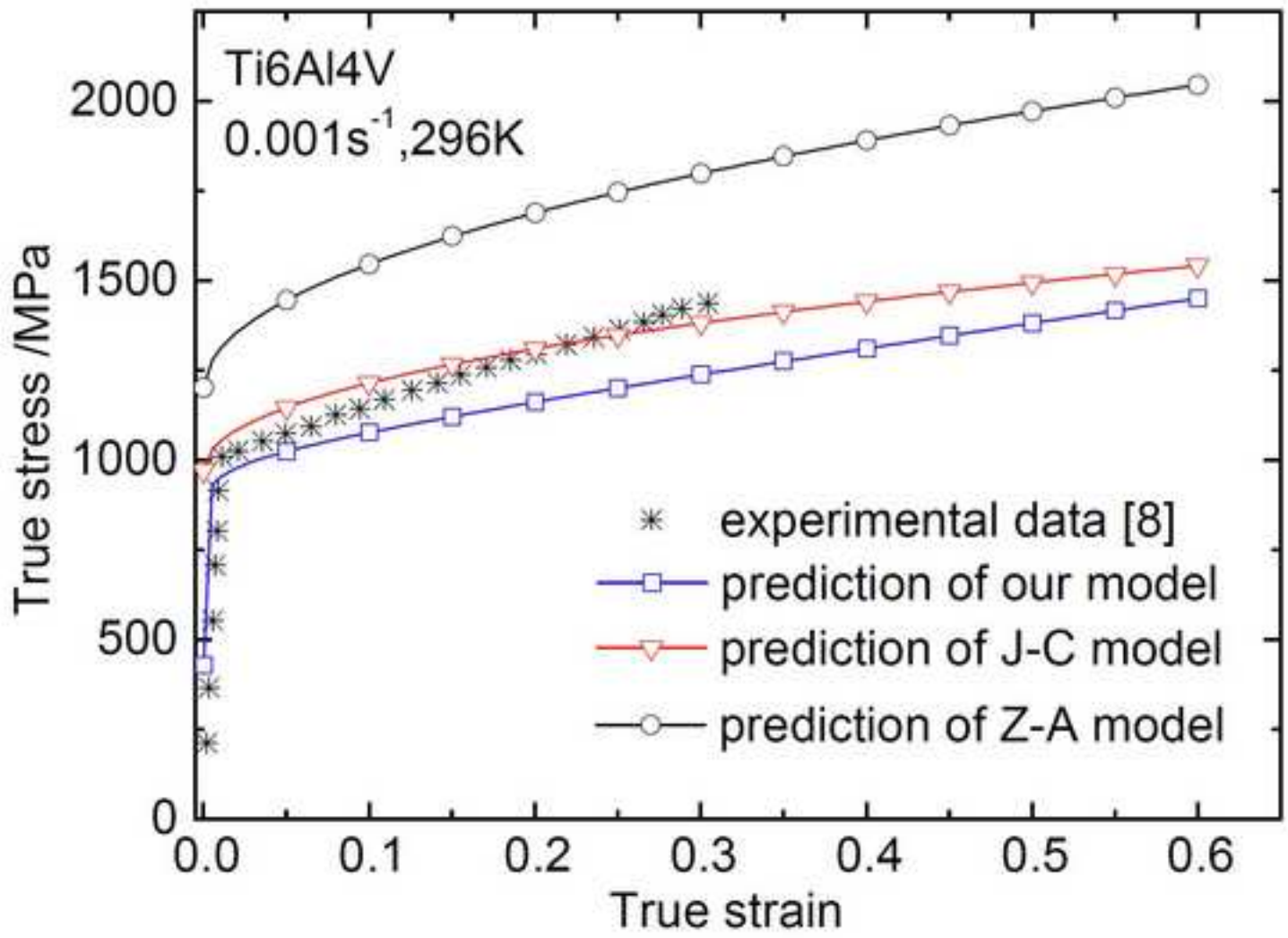

Fig. 5 Comparisons of different flow stress predictions with experimental data of TI6A14V at 0.001 s^{-1} and room temperature.

Figure(s)
Click here to download high resolution image

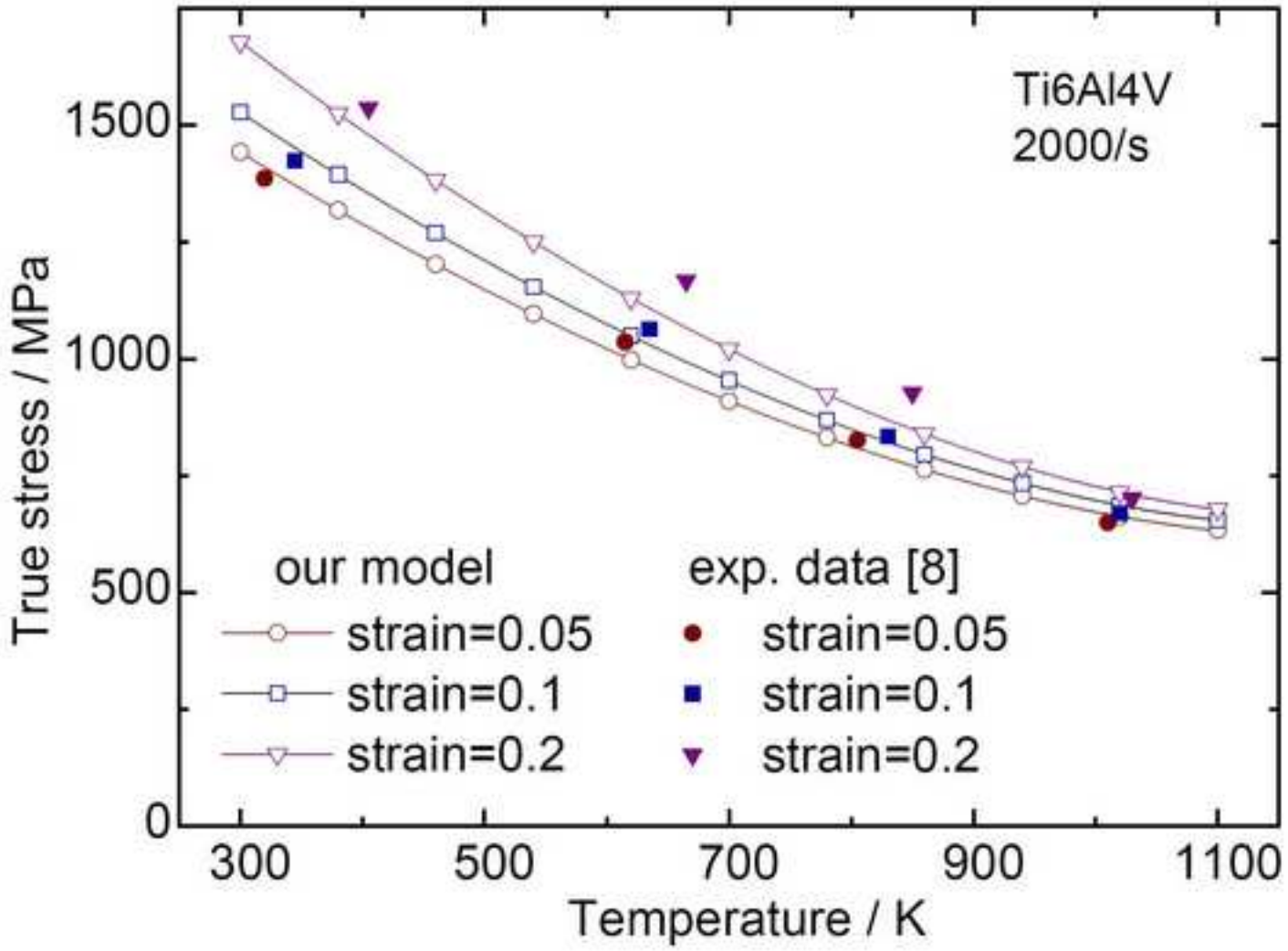

Fig. 6 Dependence of flow stress of Ti6Al4V on temperature at 2000 s^{-1} and different strains.

Figure(s)
Click here to download high resolution image

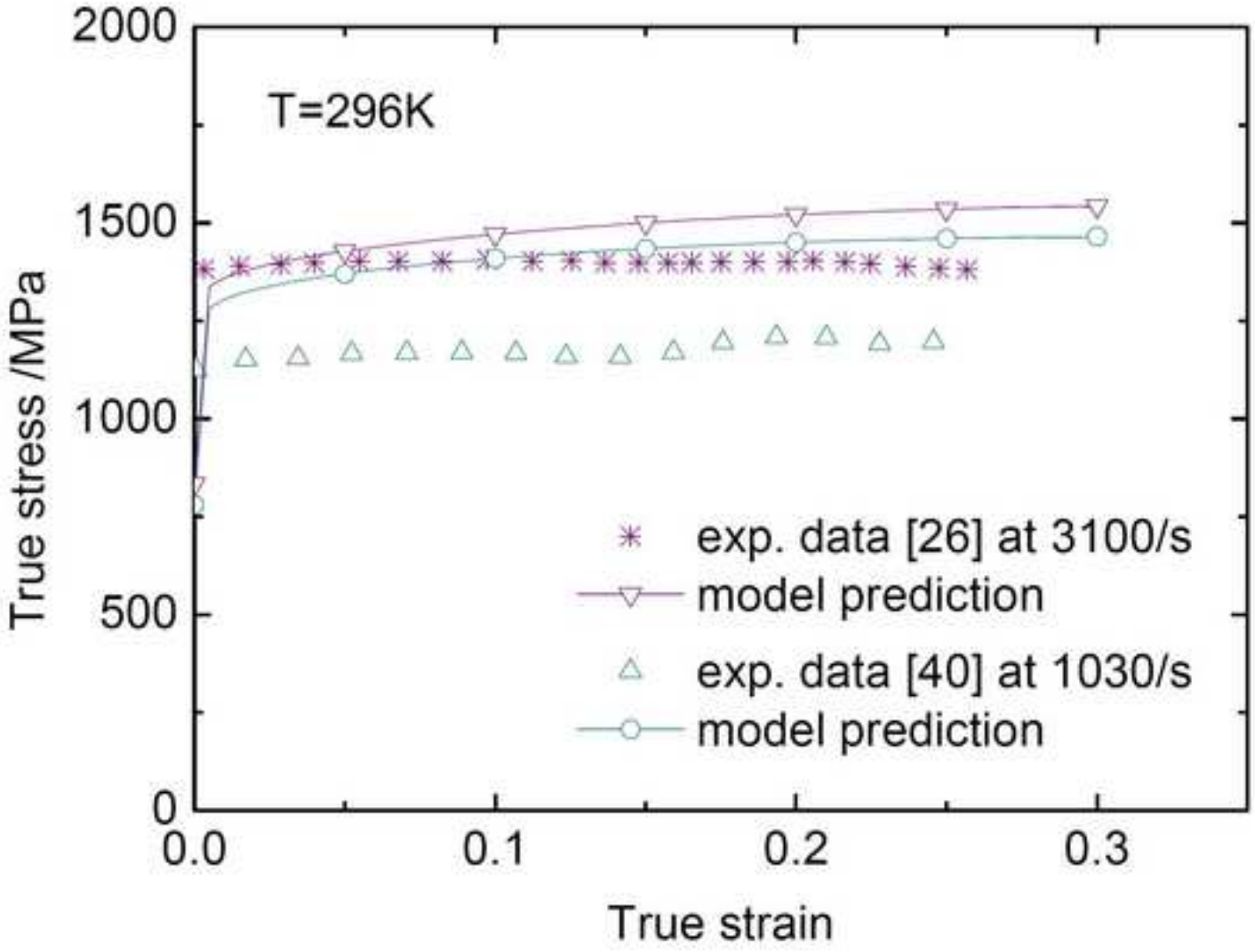

Fig. 7 Comparisons of our model predictions with others' experimental data of Ti6Al4V alloy.

Table 1 Final optimized results for constitutive parameters of Ti6A14V

Constitutive parameters	Theoretically allowed range	Optimized results	Unit
$\hat{\sigma}_{th0}$	[1000 , 2000]	1248.7	MPa
$\hat{Y}$	[1500 , 3500]	2133.7	MPa
n_1	[0, 1]	1.0	/
α	[1E-6, 1E-4]	1.0×10^{-6}	$1/K$
β	[1E-6, 1E-4]	6.0638×10^{-5}	$1/K$
p	(0, 1]	0.6	/
q	[1, 2]	1.0	/